Chapter 7

3D Holographic Millimeter-Wave Imaging for Concealed Metallic Forging Objects Detection

Lulu Wang

Additional information is available at the end of the chapter

http://dx.doi.org/10.5772/intechopen.73655

Abstract

This chapter investigates the feasibility of using 3D holographic millimeter-wave (HMMW) imaging for diagnosis of concealed metallic forging objects (MFOs) in inhomogeneous medium. A 3D numerical system, including radio frequency (RF) transmitters and detectors, various realistic MFOs models and signal and imaging processing, is developed to analyze the measured data and reconstruct images of target MFOs. Simulation and experimental validations are performed to evaluate the HMMW approach for diagnosis of concealed MFOs. Results show that various concealed objects can be clearly represented in the reconstructed images with accurate sizes, locations and shapes. The proposed system has the potential for further investigation of concealed MFOs under clothing in the future, which has the potential applications in on body concealed weapon detection at security sites or MFOs detection in children.

Keywords: holographic millimeter-wave imaging, concealed metallic object, dielectric properties, millimeter-wave, microwave imaging

1. Introduction

Imaging approaches for diagnosis of concealed metallic objects [1], such as on body weapon detection [2, 3] and metallic foreign objects (MFOs) detection in children [4], have received many attentions worldwide in recent years. Concealed weapon detection underneath human subjects' clothing is an active research topic due to rapid screening of human subjects is urgent needed at some security sites, such as airports [1]. In 1995, the United States started the concealed weapon detection program [2] to detect concealed weapons from a standoff distance, especially when it is impossible to arrange the flow of people through a controlled procedure [3].

IntechOpen

© 2018 The Author(s). Licensee IntechOpen. This chapter is distributed under the terms of the Creative Commons Attribution License (http://creativecommons.org/licenses/by/3.0), which permits unrestricted use, distribution, and reproduction in any medium, provided the original work is properly cited. CC BY

Various imaging techniques include infrared imaging [5, 6], passive millimeter-wave (MMW) imaging [7–9], active MMW imaging [10, 11], X-ray imaging [12, 13] and holographic imaging [14–17] have been investigated for concealed metallic object detection. Recent studies have demonstrated that passive MMW imaging has the most potential to become a useful tool to identify concealed MFOs under clothing [18, 19], which has been investigated for various applications include security, military, surveillance and biomedical [20].

Passive MMW imaging sensor techniques offer the best near-term potential for providing a non-invasive method of observing metallic and plastic objects concealed underneath common clothing. However, MMW cameras alone cannot provide useful information about the detail and location of the individual being monitored. The passive MMW system can produce indoor and outdoor images in bad weather, such as smoke and fog [21]. It has been applied to scan human subjects moving in an unconstrained flow, however, the MMW image has poor quality due to low-level signals and system noise [5]. In order to improve the accuracy and specificity of MMW for diagnosing concealed MFOs, many researchers aimed to develop a new MMW approach such as imaging algorithm and implement system.

Holographic technique was first applied in microwave imaging in 1948 [22]. An interference pattern between reference wave and diffracted wave (created by an object) is recorded to produce a hologram that can be digitally stored. The holograms are reconstructed by numerically synthesizing the reference wave, which is well-known wave front reconstruction processing. The target object can be reconstructed from the measured reflections and holograms. Holographic approaches are very different from the conventional synthetic aperture radar imaging method particularly in imaging geometry and no field approximations are required for holographic, which have recently been applied in MMW for MFOs detection [14, 15]. Farhat and Guard [14] applied the holographic approach for concealed weapon detection, and this technique was dramatically improved by Collins et al. [15]. The concealed MFOs detection system aims at extracting features of MFOs and reconstructing the MFOs using the measured data. The image quality is often limited by low signal-to-noise ratio and long scan time. Existing MMW methods are multi-frequency approach, which reconstruct a 3D image from a sequence of 2D images that obtained at different frequencies. However, the multi-frequency MMW methods have difficulty in practical implementations and the broadband measurements also cause large noises.

This chapter demonstrates the feasibility of using a single frequency 3D holographic millimeter-wave (HMMW) imaging system and method to detect various small MFOs in inhomogeneous medium. A computer model is developed under MATLAB environment to validate the proposed theory and measurement system setups. The system contains a HMMW measurement model and various realistic models. Simulation and experimental validations are performed to evaluate the accuracy, effectiveness and performance of the proposed theory. The remainder of this chapter is organized as follows. Section 2 introduces the 3D HMMW measure system and imaging processing. Sections 3 and 4 present simulation and experimental performances. Section 5 gives discussion and conclusion of this study.

http://dx.doi.org/10.5772/intechopen.73655

2. Methodology

2.1. Imaging measurement system

Figure 1 shows the proposed HMMW system for concealed metallic object detection. The system contains a RF generator (vector network analyzer, VNA) to illuminate microwave signals, a data acquisition unit consists of a single transmitter to transmit microwave signals into a target object and an array of receivers to measure scattered electric fields from the target object, a signal and imaging processor to analyze the measured signals which contains phase and amplitude information as well as reconstruct image of the target object using an imaging algorithm, and an image display unit to display the reconstructed image.

During data collection, port one of the VNA generates millimeter waves to the object of interest and the backscattered electromagnetic fields from the object are recorded at each receiver in the detector array plane that is connected to the second port of VNA. The distance between the target object and the data acquisition unit is in far-field region. The recorded signals include phase and amplitude information, which are used to compute the complex visibility data for each possible pair of receivers. An image of the object can be reconstructed from recorded data using the HMMW algorithm.

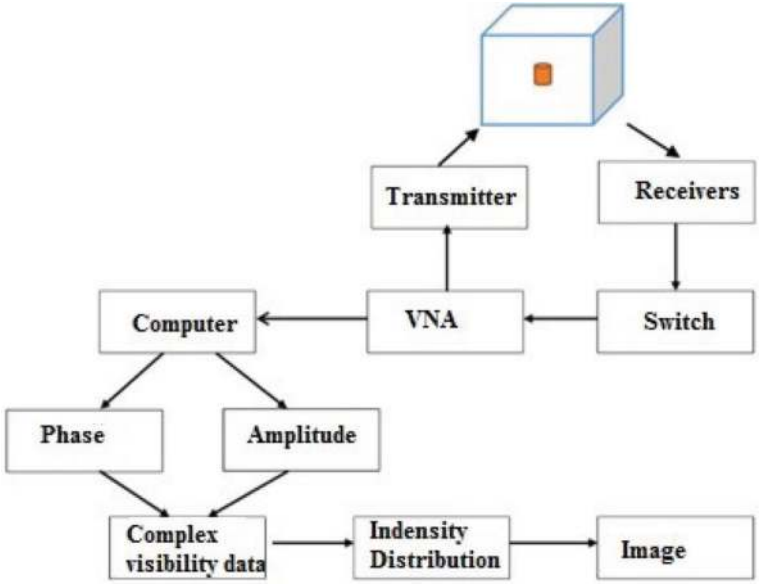

Figure 1. Experimental procedure.

2.2. Antenna part

In order to investigate the feasibility of using the 3D HMMW to detect concealed MFOs, 16 four-band patch antennas or waveguide antennas were simulated as both transmitters and detectors. **Figure 2** shows the designed four-band patch antenna with length of 10.7 mm, width of 6.3 mm, and height of 0.254 mm. As shown in **Figure 2(b)** and **(c)**, top layer and bottom layer of the proposed antenna contain 12 holes (0.15 mm in diameter) that aims to work in four broadband. The subtract material between the two layers of the antenna is RT/duriod6002 with dielectric property close to 1.

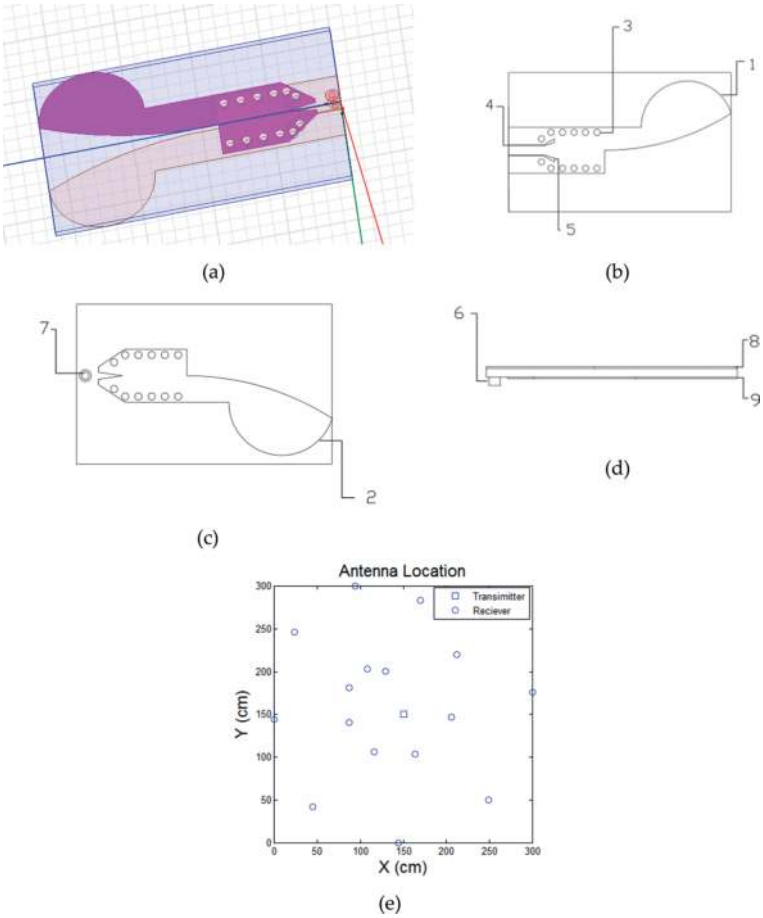

Figure 2. (a) Multiband patch antenna; (b) top layer of the designed antenna: (1) top antenna, (3) holes, (4 and 5) trumpet holes; (c) bottom layer of the antenna: (2) bottom antenna, (7) feed probe hole; (d) sideview of the antenna: (6) feed probe, (8) dielectric layer, (9) ground plate; (e) sensor array configuration.

http://dx.doi.org/10.5772/intechopen.73655

The incident electric field from each transmitter is [23]:

$$\vec{\mathrm{E}}_{inc}(R,\theta,\varnothing) = \left(-\frac{j\,k_0}{2\,\pi^2}\right)\vec{\mathrm{E}}_0\left(\frac{e^{-jk_0R_0}}{R_0}\right)ABh(\theta,\varnothing)\vec{\mathrm{P}}(\theta,\varnothing) \tag{1}$$

Where k_0 is prorogation constant of free-space, R and R_0 are the distance from the object to the detector and transmitter, respectively. $\vec{\mathrm{E}}_0$ is wave amplitude of TE10 mode at within waveguide aperture, A and B are narrow and wide aperture dimensions of antenna, respectively, h is radiation pattern, $\vec{\mathrm{P}}$ is polarization vector.

In far-field condition, the scattered electric field from the object can be computed as [24]:

$$\vec{\mathrm{E}}_{scat}(\vec{\mathrm{r}}) = \left(\frac{k_0^2}{4\pi}\right)\int_V\left(\varepsilon(\vec{s})-\varepsilon_0\right)\vec{\mathrm{E}}_{inc}(\vec{s})\,\frac{e^{-jk_0R}}{R}\,dV \tag{2}$$

Where $\varepsilon(\vec{\mathrm{s}})$ and ε_0 are the complex relative permittivity of object and free-space, respectively. R means the distance between the object and the detector.

2.3. Signal and imaging processing

As shown in **Figure 3**, a point Q is located within a 3D object, the visibility for any two detectors located at $\vec{r}_i$ and $\vec{r}_j$ can be computed [25]:

$$\vec{V}_{ij} = < \vec{E}_{scat}\left(\vec{r}_i\right)\cdot\vec{E}^{*}_{scat}\left(\vec{r}_j\right) > \tag{3}$$

Where * is the complex conjugate and < > denotes time average.

The total visibility data can be computed as:

$$\vec{V} = \sum_{i}^{N}\vec{V}_{ij},\, N \geq 3, i \neq j \tag{4}$$

Define the object intensity distribution at position $\vec{s}$ as [26]:

$$I(\vec{s}) = \left(\frac{k_0^2}{4\pi}\right)^2\left|\varepsilon(\vec{s})-\varepsilon_0\right|^2\vec{\mathrm{E}}_T(\vec{s})\cdot\overrightarrow{\mathrm{E}^{*}_T}(\vec{s}') \tag{5}$$

All detectors are located on the same plane, thus, define the line integral as:

$$\tilde{I}(l,m) = \int_s\frac{I(s,l,m)}{\sqrt{1-l^2-m^2}}\,ds \tag{6}$$

Where $l = sin\theta cos\phi$ and $m = sin\theta sin\phi$. $u = \left(\left(\vec{x}_j\right)-\left(\vec{x}_i\right)\right)/\lambda_0$, $v = \left(\left(\vec{y}_j\right)-\left(\vec{y}_i\right)\right)/\lambda_0$, λ_0 means the wavelength of free-space.

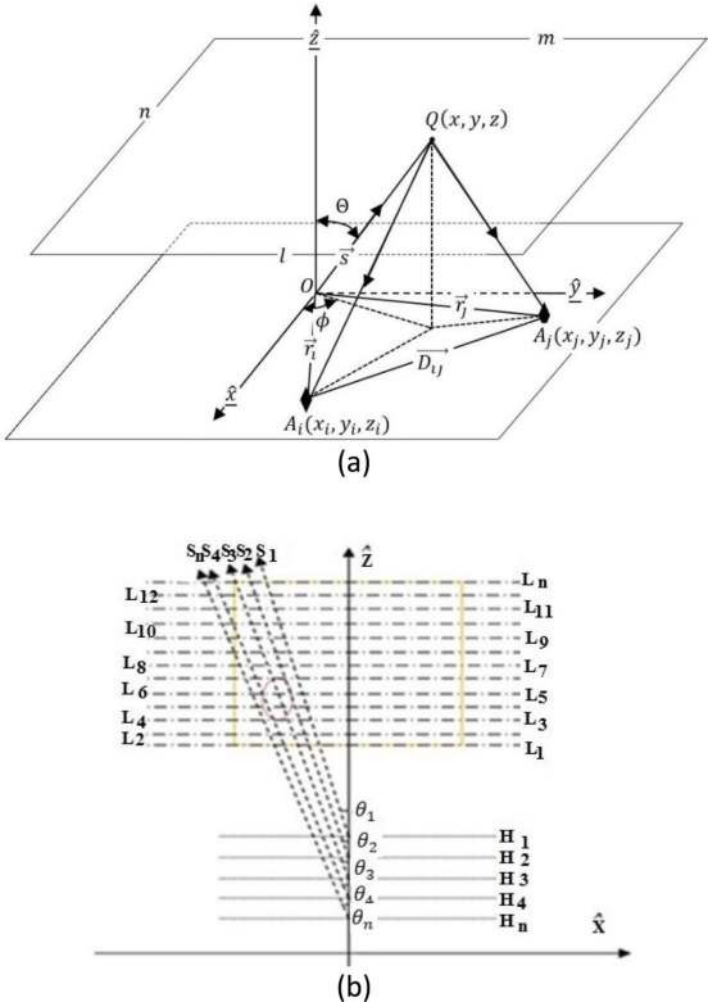

Figure 3. (a) Geometry of two detectors, (b) scattering characterization scheme from different receiving height *H* [24].

A 2D image is obtained by using inversion Fast Fourier Transformation:

$$\tilde{I}(l,m) = \iint V(u,v)\, e^{j2\pi(ul+vm)}\, dldm \tag{7}$$

The 2D image difference between each two 2D images is computed by differentiating 2D images when the sensor array plane is placed at different heights (H):

$$I(H = z_n, l, m) = d\tilde{I}(l,m) \cdot (1 - l^2 - m^2)/dz \tag{8}$$

$$d\tilde{I}/dz = \left(\tilde{I}_{Z_n} - \tilde{I}_{Z_{n-1}}\right)/(Z_n - Z_{n-1}) \tag{9}$$

http://dx.doi.org/10.5772/intechopen.73655

Where $z_n = s_n(\cos\theta_n)$, θ_n is the receiving angle of the position s_n with the sensor plane placed at the selected height H_n (**Figure 3(b)**).

A 3D image can be reconstructed by acquiring the measured 2D intensity distributions when the sensor array plane is placed at different vertical locations, and computing a sequence of 2D images, $\tilde{I}_{z_n}$.

3. Simulation

A numerical system was developed under MATLAB environment to investigate the proposed theory and system for diagnosing concealed MFOs. An array of 16 open-ended waveguide antennas with one element for transmitter and others for receivers. The target object was located at $z = 0$ mm and it was assumed to be fully contained in a rectangle imaging domain with length of 300 mm. The sensor array plane was placed at $z = -200$ m. Five models (see **Figure 4**) were developed using the published dielectric properties to evaluate the 3D HMMW [27].

Model I was made of two metallic spheres (10 mm in diameter, $x_1 = 0, y_1 = 0, z_1 = 35$, $x_2 = 50, y_2 = 0, z_2 = 35$) embedded in a cylindrical tank (240 mm in diameter and 70 mm in height) filled of clothing material; Model II was made of two wood spheres (5 mm in diameter, $x_1 = 0, y_1 = 0, z_1 = 35$) embedded in a cylindrical tank; Model III was made of two wood

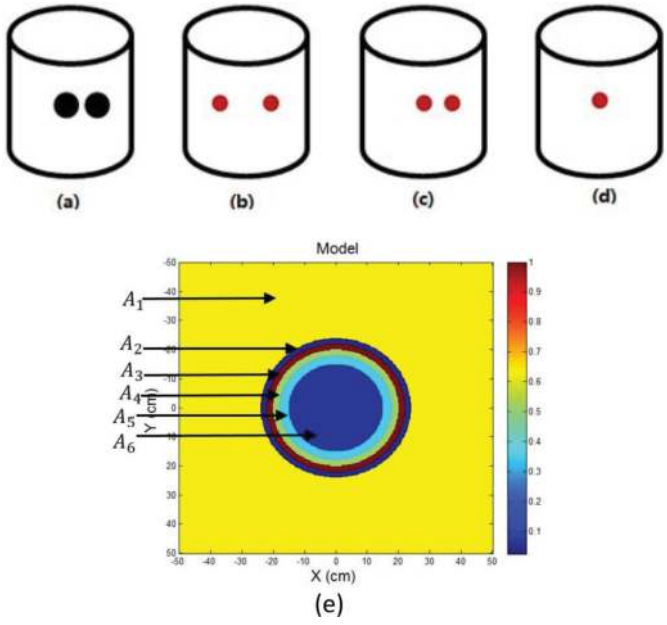

Figure 4. (a) Model I, (b) Model II, (c) Model III, (d) Model IV, (e) Model V (A 1: matching medium, A 2: cloth, A 3: metallic object, A 4: skin, A 5: skull, A 6: fat).

spheres (10 mm in diameter, $x_1 = 0, y_1 = 0, z_1 = 35$, $x_1 = 20, y_1 = 0, z_1 = 35$) embedded in a cylindrical tank; Model IV was made of one metallic sphere (10 mm in diameter, $x_1 = 0$, $y_1 = 0, z_1 = 35$) embedded in a cylindrical tank.

To investigate the feasibility of on body conceded weapon detection using the proposed imaging method, a Model V includes human phantom was developed using published dielectric properties of various tissues, and a series of simulations were carried out on a personal computer by the developed computer model. **Figure 4(e)** shows the Model V, where the multimedia dielectric object (cylinder) was located at z = 0 mm and it was assumed to be fully contained in a rectangle imaging domain with length 100 cm. This multimedia object simulates human body (contains skin, skull and fat), clothing and metallic object. The scale values of the published dielectric properties of real tissues were applied (see **Table 1**).

Figure 5 shows the reconstructed images of Model I at different frequencies in water. Both cylindrical box and two metallic objects are clearly identified in the frequency range of 20–25 GHz, but only metallic object is identified when frequency out of this range.

Figure 6 shows the reconstructed images of Model II when the two objects located at different distance with frequency of 23 GHz in free-space. Results show that two small wood spheres are successfully identified when the distance between the two items great than 3 mm.

Figure 7 shows the 3D reconstructed images of Model III and Model IV when the sensor array plane moved from $z = -650$ mm to $z = -600$ mm in 50 equal steps at frequency of 23 GHz.

To simulate on body weapon detection using the HMMW approach, the image measuring system was set-up in free-space with operating of frequency at 96 GHz, a 16-element antenna array plane was placed at the bottom of the model with a distance of 65 cm. A small four-band patch RF antenna was designed as transmitter and receiver and it was simulated using HFSS software with operating frequency of 50–120 GHz. **Figure 8** shows the return loss of the four-band patch antenna, which has the ability to receive good result at 96–116 GHz.

Figure 9 shows the 2D reconstructed images of Model V at operating frequency of 96 GHz. The rectangle imaging region contains the dielectric object (human model with clothing) and the steel stainless object. Simulation result demonstrates that the metallic object underneath

No	Region	Dielectric properties		Scale value of dielectric properties	
		ε_r	σ (S/m)	ε_r	σ (S/m)
A4	Skin	41	4	0.5125	0.4
A5	Skull	25	2	0.31	0.2
A6	Fat	5	0.4	0.06	0.04

Table 1. Dielectric properties of human body [26].

http://dx.doi.org/10.5772/intechopen.73655

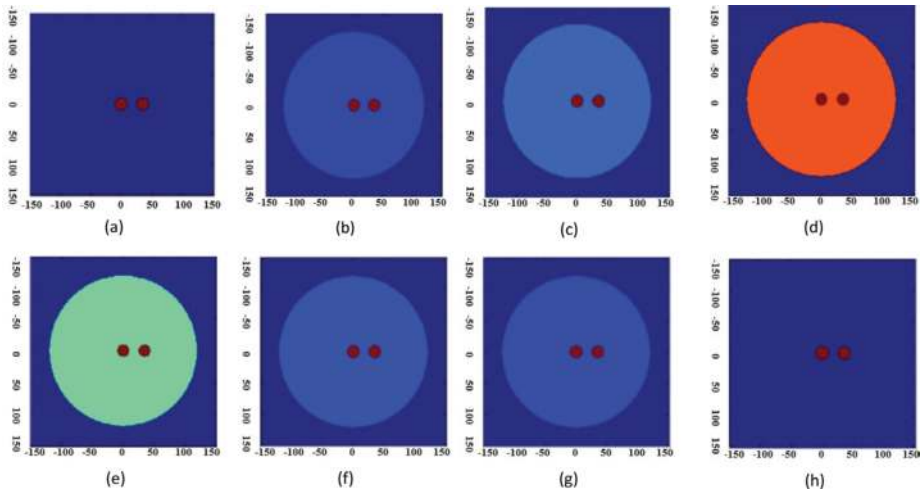

Figure 5. Reconstructed images of Model I with operating frequency of (a) 19 GHz, (b) 20 GHz, (c) 21 GHz, (d) 22 GHz, (e) 23 GHz, (f) 24 GHz, (g) 25 GHz, (h) 26 GHz.

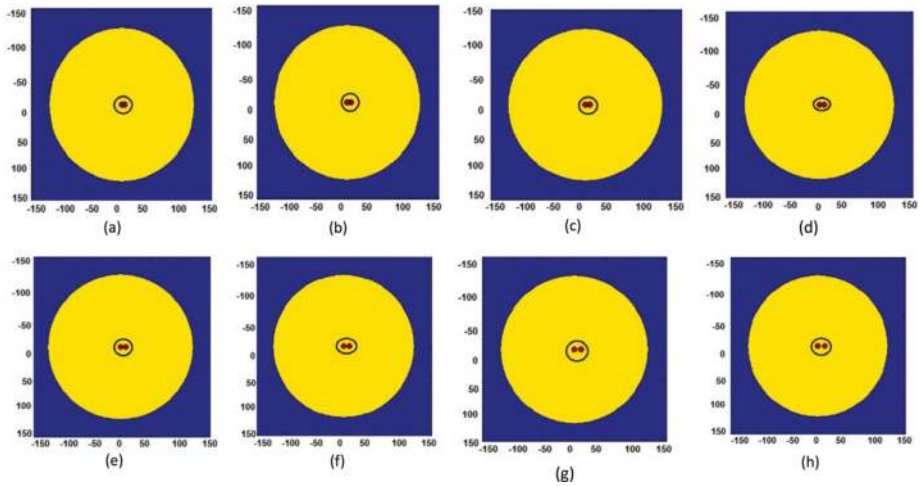

Figure 6. Reconstructed images of Model II when the distance between two wood spheres is: (a) 0 mm, (b) 1 mm, (c) 2 mm, (d) 3 mm, (e) 4 mm, (f) 5 mm, (g) 6 mm, (h) 7 mm.

wof human model's clothing has been successfully imaged, and structures of the tested human model are clearly identified with operation frequency of 96 GHz. Color bar plots signal energy on a linear scale, normalized to the maximum in the image space and values below 0.1 are rendered as blue.

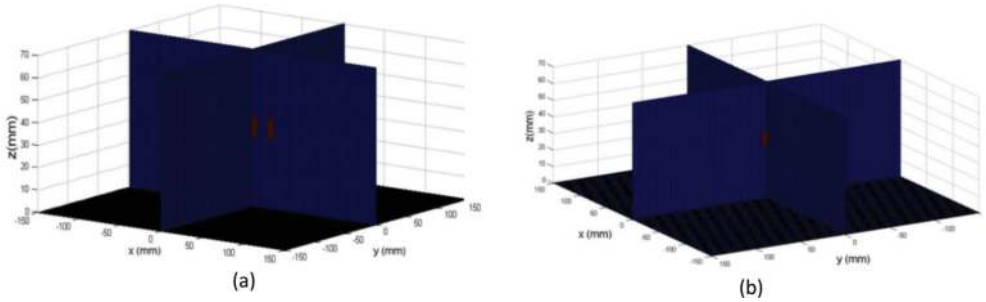

Figure 7. (a) 3D reconstructed image of Model III, (b) 3D reconstructed image of Model IV.

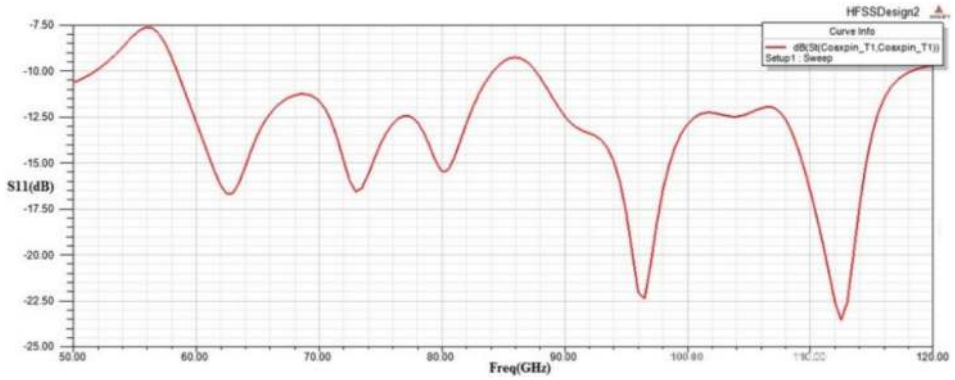

Figure 8. Simulated S11 value of the designed 4-band patch antenna.

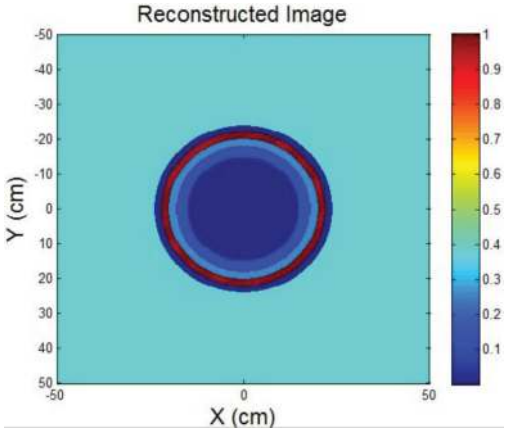

Figure 9. Reconstructed 2D image of Model V.

http://dx.doi.org/10.5772/intechopen.73655

4. Experimental validation

An experimental study was conducted to evaluate the 3D HMMW system for concealed MFO detection (see **Figure 10**). A concealed steel ball (10 mm in diameter) embedded in a plastic box (100 × 100 × 40) mm^3 that filled of emulsifying wax (see **Figure 10(c)**). An array of 16 open-ended waveguide antennas with one element for transmitter and others for receivers. The plastic box was placed at $z = 0$ mm, and the sensor array plane was moved from $z = -600$ mm to $z = -560$ mm in 40 equal steps during data collection. During data collection, the VNA excited MMW signals to each transmitter located on the sensor array at frequency of 23 GHz. The scattered signals from the target object were measured by each detector. 2D and 3D images of the target object were reconstructed using the proposed imaging algorithms (as detailed above).

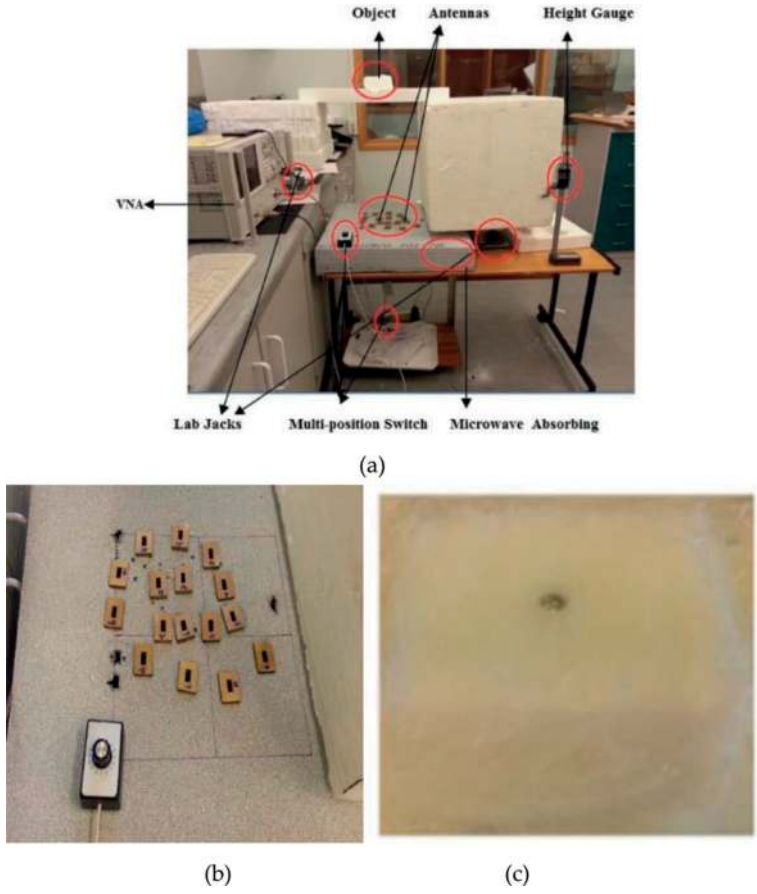

Figure 10. (a) HMMW measurement setup; (b) sensor array; (c) target object.

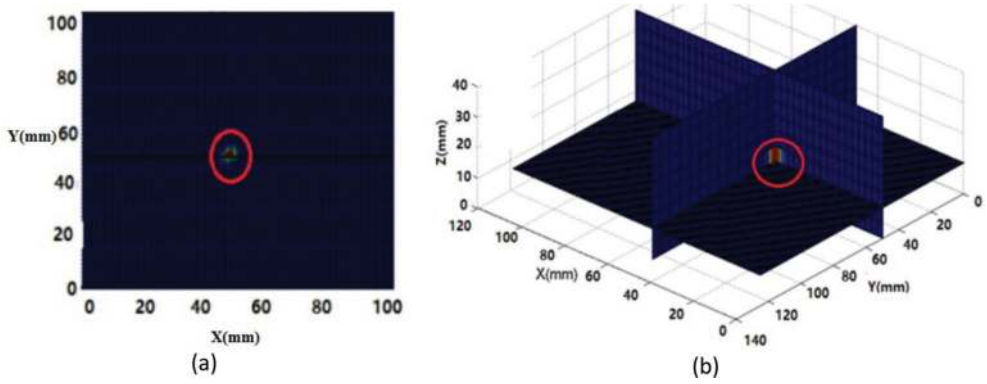

Figure 11. (a) 2D reconstructed image of concealed steel ball, (b) 3D reconstructed image of concealed steel ball.

Figure 11 shows the 2D and 3D reconstructed images of the concealed metallic steel ball. The steel ball is clearly identified in the reconstructed images with correct location, shape and size.

5. Conclusions

This chapter investigated the 3D HMMW method for various concealed objects detection and the theory has been evaluated through numerical and experimental validations. It was found that various small concealed metallic and wood objects with different sizes and locations can be identified in the reconstructed HMMW images. Results showed that the proposed HMMW has the potential for investigating characterization and structure of concealed objects. The potential applications of the 3D HMMW include on body weapon detection and packed food quality control.

Acknowledgements

The author gratefully acknowledges the financial supports from the National Natural Science Foundation of China (Grant No. 61701159, JZ2017GJQN1131), the Natural Science Foundation of Anhui Province (Grant No. 101413246, JZ2017AKZR0129), the Foundation for Oversea Master Project from the Ministry of Education of the People's Republic of China (Grant No. 2160311028), and the start-up funding from the Hefei University of Technology (Grant No. 407037164).

Conflict of interest

The author declares no conflict of interest.

Author details

Lulu Wang[1,2]*

*Address all correspondence to: luluwang2015@hfut.edu.cn

1 School of Instrument Science and Opto-electronics Engineering, Hefei University of Technology, Hefei, China

2 Institute of Biomedical Technologies, Auckland University of Technology, Auckland, New Zealand

References

[1] Gianesin B, Zefiro D, Paparo F, Caminata A, Balocco M, Carrara P, et al. Characterization of ferromagnetic or conductive properties of metallic foreign objects embedded within the human body with magnetic iron detector (mid): Screening patients for MRI. Magnetic Resonance in Medicine. 2015;**73**(5):2030-2037

[2] Appleby R, Wallace HB. Standoff detection of weapons and contraband in the 100 GHz to 1 THz region. IEEE Transactions on Antennas & Propagation. 2007;**55**(11):2944-2956

[3] Bavirisetti DP, Dhuli R. Two-scale image fusion of visible and infrared images using saliency detection. Infrared Physics & Technology. 2016;**76**:52-64

[4] Nation J, Jiang W. The utility of a handheld metal detector in detection and localization of pediatric metallic foreign body ingestion. International Journal of Pediatric Otorhinolaryngology. 2017;**92**:1

[5] Chen HM, Lee S, Rao RM, Slamani MA, Varshney PK. Imaging for concealed weapon detection: A tutorial overview of development in imaging sensors and processing. IEEE Signal Processing Magazine. 2005;**22**(2):52-61

[6] Zhu JZ, Zhang CS, Feng FZ, Min QX, Chao X. Study on probability of detection for fatigue cracks in sonic infrared imaging. Infrared Physics & Technology. 2006;**77**:296-301

[7] Shi X, Yang MH. Development of passive millimeter wave imaging for concealed weapon detection indoors. Microwave & Optical Technology Letters. 2014;**56**(7):1701-1706

[8] Kemp MC. Millimetre wave and terahertz technology for the detection of concealed threats: A review. International Society for Optics and Photonics. 2006;**6402**:10-19

[9] Farsaei AA, Mokhtari-Koushyar F, Seyed-Talebi SM, Kavehvash Z, Shabany M. Improved two-dimensional millimeter-wave imaging for concealed weapon detection through partial Fourier sampling. Journal of Infrared, Millimeter, and Terahertz Waves. 2016;**37**(3):267-280

[10] Du K, Wang W, Nian F, Chen W, Hu FJ. Concealed objects detection in active millimeter-wave images. Systems Engineering & Electronics. 2016;**38**(6):1463-1469

[11] Grossman EN, Miller AJ. Active millimeter-wave imaging for concealed weapons detection. Proceedings of SPIE - The International Society for Optical Engineering. 2003;**5077**: 62-70

[12] Smith GJ. Detection of contraband concealed on the body using x-ray imaging. Human Detection & Positive Identification Methods & Technologies. 1997;**2932**:115-120

[13] Jannson T, Gertsenshteyn M. Hard X-ray focusing optics for concealed object detection. Proceedings of SPIE. 2006;**6213**:2-12

[14] Farhat NH, Guard WR. Millimeter wave holographic imaging of concealed weapons. Proceedings of the IEEE. 1971;**59**(9):1383-1384

[15] Collins DH, Mcmakin DL, Hall TE, Gribble PR. Real-time holographic surveillance system. 1995; US patent, US5455590

[16] Zhao Y, Wang Z, Jiang Z. Digital holographic imaging for diffuse-reflection metal surface with strong feature. In: International Symposium on Optoelectronic Technology and Application. 2016; 101553V

[17] Sheen DM, Collins DH, Hall TE, Mcmakin DL, Gribble PR, Severtsen RH. Real-time wideband holographic surveillance system. 1996; US Patent, US5557283

[18] Nagayama Y, Ito N, Kuwahara D, Tsuchiya H, Yamaguchi S. Development of 2-d horn-antenna millimeter-wave imaging device (HMID) for the plasma diagnostics. Review of Scientific Instruments. 2017;**88**(4):1647

[19] Alotaibi NN, Hamdi KA. Switched phased-array transmission architecture for secure millimeter-wave wireless communication. IEEE Transactions on Communications. 2016; **64**(3):1303-1312

[20] Hu F, Cheng Y, Gui L, Wu L, Zhang X, Peng X, et al. Polarization-based material classification technique using passive millimeter-wave polarimetric imagery. Applied Optics. 2016;**55**(31):8690

[21] Hung CY, Weng MH, Yang RY, Wu HW. Design of a compact CMOS bandpass filter for passive millimeter-wave imaging system application. Journal of Electromagnetic Waves & Applications. 2009;**23**(17-18):2323-2330

[22] Kock WE. Microwave holography. In: Engineering Applications of Lasers and Holography. US: Springer; 1975

[23] Silver S. Microwave antenna theory and design. P. Peregrinus on behalf of the Institution of Electrical Engineers. 1984. pp. 87-90

[24] Wang L, Al-Jumaily AM, Simpkin R. Imaging of 3-D dielectric objects using far-field holographic microwave imaging technique. Progress in Electromagnetics Research B. 2014;**61**:135-147

[25] Levanda R, Leshem A. Synthetic aperture radio telescopes. IEEE Signal Processing Magazine. 2010;**27**:14-29

[26] Wang L, Al-Jumaily AM, Simpkin R. Holographic microwave imaging for medical applications. Journal of Biomedical Science & Engineering. 2013;**6**(8):823-833

[27] Born M, Wolf E. Principles of Optics: Electromagnetic theory of propagation, interference and diffraction of light. Cambridge University Press. 2000